DE GRUYTER OPEN

*Journal of* ELECTRICAL ENGINEERING, VOL 67 (2016), NO5, 365–370

# INFLUENCE OF QUENCHING RATE ON THE STRUCTURE, MORPHOLOGY, AND HYPERFINE PARAMETERS OF AMORPHOUS RIBBONS

**Narges Amini** [*,**] — **Július Dekan** [*] — **Milan Pavúk** [*] — **Safdar Habibi** [**] — **Marcel Miglierini** [***]

In this work, an amorphous alloy with the nominal composition of $Fe_{78}Si_9B_{13}$ was produced by a melt spinning method. Using different velocities of a quenching cooper wheel enabled us to study the influence of quenching rate upon the structural characteristics of the resulting ribbons. Structural features of the samples were checked by Mössbauer spectroscopy and X-ray diffraction. The latter performed in a grazing angle geometry enabled us to explore both sides of the as-quenched ribbons. The onset of crystallization was estimated by differential scanning calorimetry (DSC) measurements. Surface features of the ribbons were examined by Scanning Electron Microscopy (SEM). In order to observe structural relaxation phenomena the samples were annealed below the onset of crystallization at 450 °C for 1 hour in Ar protective atmosphere. Even though the annealed ribbons are still amorphous relevant changes were observed in their hyperfin parameters as derived from Mssbauer spectrometry.

K e y w o r d s: amorphous alloys, XRD, DSC, SEM, Mössbauer spectrometry, heat treatment

## 1 INTRODUCTION

Iron-based metallic glasses (MGs) exhibit excellent soft magnetic behaviour coupled with good mechanical properties. Therefore they have been widely studied during several decades [1, 2]. Due to lack of boundary grains in their structures this type of materials has some advantages in comparison with crystalline alloys of the same composition. They have been studied from different aspects such as magnetic properties, structural arrangement, mechanical properties, and progress of crystallization by different tools as X-ray diffraction (XRD), differential scanning calorimetry (DSC), Mssbauer spectrometry, Hall and electrical resistivity measurements, *etc* [3, 4].

Ok and Morrish [5] have found that surface crystallization on the wheel (dull) side of $Fe_{82}B_{12}Si_6$ MG ribbons precedes the bulk crystallization transformation from as-quenched amorphous to crystalline state using both transmission Mössbauer spectrometry and scattering Mössbauer spectroscopy. Similar results were found by these authors also for $Fe_{75.4}B_{14.4}Si_{10.4}$ MG [6]. Nevertheless, as it was shown in [7, 8], both sides of Fe-Nb-B ribbons exhibit different properties due to provoked crystallization in a very thin layer at the wheel side surface. The obtained parameters of coercive fields are different for the wheel and air (shiny) sides. Also several studies have focused on the $Fe_{78}Si_9B_{13}$ MGs [9, 10]. Moreover in some studies, Mössbauer spectrometry was employed to seek for correlation between the quenching wheel velocity and magnetic anisotropy of $Fe_{78}Si_9B_{13}$ MGs [1, 3, 11].

The above mentioned points motivated us to consider $Fe_{78}Si_9B_{13}$ MGs prepared under different production velocity conditions. To the authors' knowledge the previous studies did not explore the effects of quenching wheel velocity upon magnetic and structural properties of $Fe_{78}Si_9B_{13}$ amorphous ribbons by Mössbauer spectrometry. MG with the same composition was investigated from the point of view of its microstructure, magnetism, and electrochemical properties by various methods [12] using samples which were prepared in a vacuum and air atmosphere with several quenching rates namely 14.6, 25.6, and 36.6 m/s. In our work, we have extended the range of quenching rates and introduced also heat treatment to modify structural properties of the investigated MG. Correlation between structural arrangement and hyperfine parameters is looked for by Mössbauer spectrometry.

## 2 EXPERIMENTAL DETAILS

Iron-based metallic glass with the nominal composition of $Fe_{78}Si_9B_{13}$ was fabricated by a melt spinning method in argon atmosphere in a form of ribbons using various linear wheel velocities namely 15, 20, 25, 30, 35, and 40 m/s. The resulting ribbons were $\sim$ 1 mm wide. Their thickness was measured by a micrometer with an accuracy of 0.001 mm.

X-ray diffraction measurements were performed by Burker D8 Discover diffractometer employing filtered Cu-$K_\alpha$ radiation. Mössbauer spectra were collected at

[*] Slovak University of Technology in Bratislava, Faculty of Electrical Engineering and Information Technology, Institute of Nuclear and Physical Engineering, Ilkovičova 3, 812 19 Bratislava, Slovakia, [**] Department of Physics, Bu-Ali Sina University, Hamedan, Iran, [***] Department of Nuclear Reactors, Czech Technical University in Prague, V Holešovičkách 2, 180 00 Prague, Czech Republic

DOI: 10.1515/jee-2016-0052, Print (till 2015) ISSN 1335-3632, On-line ISSN 1339-309X 

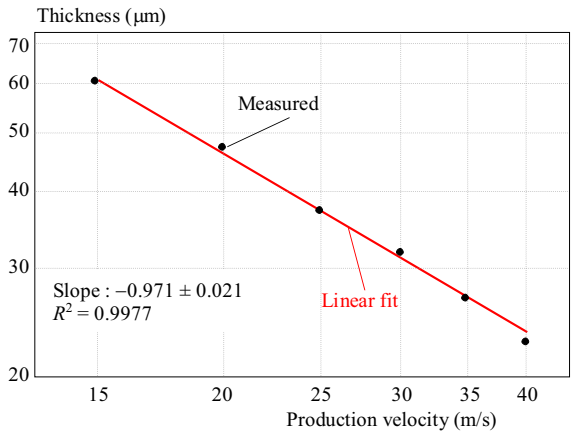


**Fig. 1.** Thickness of the MG ribbons plotted against velocity of the quenching wheel, logarithmic scales

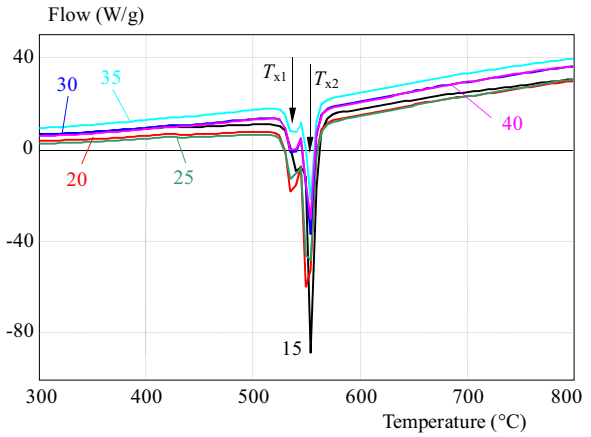


**Fig. 2.** DSC thermograms of as-quenched amorphous alloys produced with the indicated velocities (in m/s)

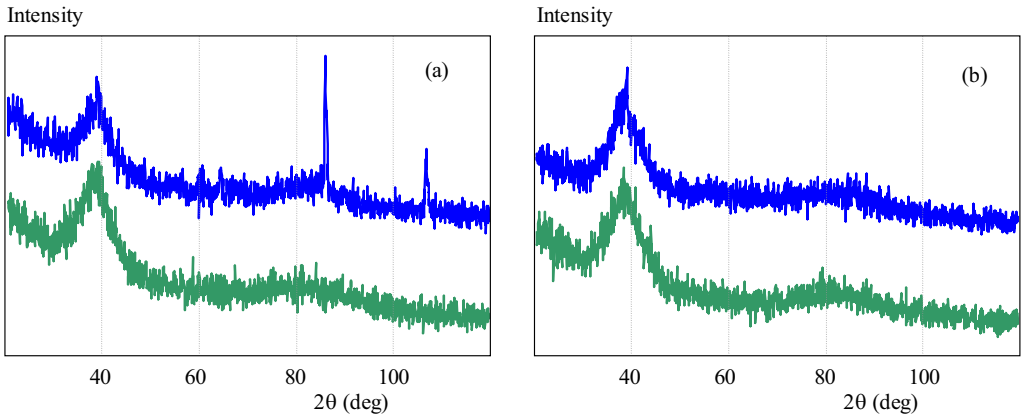


**Fig. 3.** (a) — XRD patterns taken from the wheel, and (b) — the air side of the $Fe_{78}Si_9B_{13}$ ribbons produced with the lowest (15 m/s – upper parts) and the highest (40 m/s – lower part) velocity. The narrow reflections are assigned to $\alpha$-Fe and $F_3Si$ nanocrystals.

**Table 1.** The temperatures corresponding to exothermic effects for the $Fe_{78}Si_9B_{13}$ MGs, $T_x$: Initiation temperature of crystallization

| Production velocity | $T_{x1}$(°C) | $T_{x2}$(°C) |
|---|---|---|
| 15 | 513.99 | 543.77 |
| 20 | 513.99 | 543.78 |
| 25 | 518.97 | 543.79 |
| 30 | 518.95 | 543.77 |
| 35 | 518.93 | 543.75 |
| 40 | 519.00 | 543.82 |

room temperature in transmission geometry using a conventional constant-acceleration spectrometer equipped with a $^{57}$Co $\gamma$-ray source in a rhodium matrix. Velocity calibration was performed by an $\alpha$-Fe foil. Mössbauer spectra were analyzed by least-square fitting procedure using the NORMOS fitting software [13]. The spectra were evaluated by Lorentzian line sextets employing distributions of hyperfine magnetic fields $P(B)$. Magnetic anisotropy of $^{57}$Fe resonant atoms was characterized by measuring the relative ratios of the 2$^{nd}$ and the 5$^{th}$ lines of the sextets.

Surface features of the ribbon prepared with the velocity of 15 m/s were checked at the wheel side by the method of Conversion Electron Mössbauer Spectrometry (CEMS). This method provides information by recording conversion electrons of all energies emitted from scanning depths down to $\sim 200$ nm.

A scanning electron microscope from Hitachi, model SU3500 was employed to provide topographic views of the investigated samples. The onset of crystallization was derived by performing DSC at a heating rate of 10 °C/min. Annealing of the prepared samples was performed at 450 °C for 60 min in the Ar protective atmosphere.

## 3 RESULTS AND DISCUSSION

### 3.1 Thickness of the ribbons

Thickness of the as-quenched ribbons is depicted in Fig. 1 as a function of the production velocity. It decreases monotonically with increasing wheel velocity so that at the maximum velocity it is almost 3 times smaller than that at the minimum one. The experimental points have been fitted with the theoretical function of $d = V^{-1}$, where $d$ is the samples thickness and $V$ denotes velocity.

The obtained theoretical fit agrees reasonably well with the expected hyperbolic behaviour providing a slope of $-0.9971$ as compared to $-1.0$ from the theoretical dependence. The correlation factor is 0.9977.

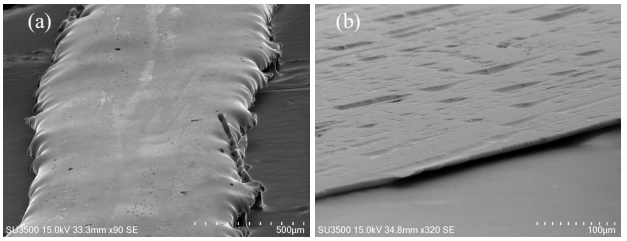


**Fig. 4.** SEM images of the produced samples with: (a) — 15 m/s, and (b) — with 40 m/s

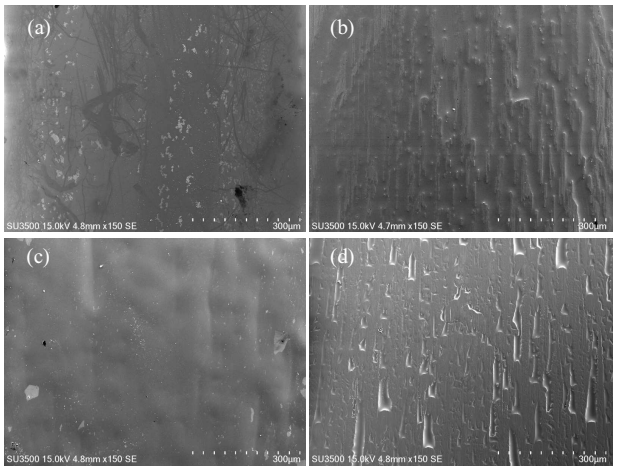


**Fig. 5.** SEM images of as-quenched state of samples with: (a), (b) — 15 m/s, and (c), (d) — with 40 m/s (a), (c) — corresponding to the air side, and (b), (d) — to the wheel side

### 3.2 DSC measurements

As illustrated in Fig. 2 two exothermic peaks can been observed for all ribbons. They indicate two crystallization steps that occur during the crystallization process.

The temperatures corresponding to the onset of the first $T_{x1}$ and the second $T_{x2}$ crystallization are collected in Table 1. They indicate that the first crystallization takes place at lower temperature in the case of samples produced with low velocities, namely 15 and 20 m/s, than for the other velocities. The second crystallization is independent on the production velocity.

### 3.3 XRD measurements

XRD patterns of the samples produced with the lowest and the highest velocity, namely 15 and 40 m/s are illustrated in Fig. 3. It has been revealed that the wheel side of as-quenched state of the former ribbon is not fully amorphous. Some signs of narrow reflections were unveiled at the Bragg angles of $2\theta = 44.5$, 65, 82.5 and 99°. Since in the studied MGs Si and B atoms are surrounded only by Fe atoms and the correlations Si–Si, Si–B, and B–B are likely bridged by them and because the Fe–Si bonding is stronger than the Fe–B one a $DO_3$-type Fe,Si solid-solution-like structure should nucleate more easily from the amorphous matrix [14]. We attributed the crystalline peaks to the presence of bcc $\alpha$-Fe and $Fe_3Si$ phases. Since only this side of the investigated sample contributes to the diffracted intensity by the above mentioned peaks only one surface is partially crystallized whereas bulk parts and the remaining surfaces are fully amorphous as evidenced by broad peaks at $2\theta = 45°$ in all patterns.

### 3.4 Scanning electron microscopy (SEM)

SEM investigations showed remarkable differences between the edges of the as quenched ribbons produced by the highest and the lowest velocity. As it can be seen in Fig. 4(a) the edges of the ribbon prepared with 15 m/s are not straight. This is caused probably by low cooling rate since during the solidification process the liquid has enough time to spread more to the sides. On contrary, the edges of the sample prepared with 40 m/s in Fig. 4(b) are smoother and sharper than those of the above mentioned sample.

Higher magnification used in Fig. 4(b) has revealed a presence of air pockets that are formed on this side of the ribbons. They originate from evaporated humidity contained in the surrounding atmosphere when the latter is trapped between the quenching wheel and the melt. Consequently, the wheel side of the ribbons is not as smooth as the opposite, *ie* the air one. More details are visible in Fig. 5 where both air and wheel sides of the ribbons prepared with highly distinct velocities are presented. All images in this figure were taken with the same magnification.

The following observations can be noted. Air sides of both the ribbons prepared with 15 m/s and 40 m/s velocity exhibit very smooth surfaces. Nevertheless, some island-type features are seen in Fig. 5(a) and to smaller extent also in Fig. 5(c). They can be hardly attributed to crystalline phases as there is no indication of the latter in the corresponding XRD patterns in Fig. 3(b). Some lines are also visible in Fig. 5(a) which might perhaps represent mechanical scratches.

Notable differences are found on the wheel sides. While for the 15 m/s prepared ribbon the whole inspected surface in Fig. 5(b) exhibits rather homogeneously rough surface, individual well separated air pockets are nicely seen in Fig. 5(d) where the wheel side of the ribbon prepared with the velocity of 40 m/s is displayed. Their isolation is presumably due to higher production velocity which limits agglomeration of gas bubbles during the quenching. Sohrabi *et al* [15] have detected the same situation in the case of $Fe_{71}Si_{13.5}B_9Nb_3Cu_1Al_{1.5}Ge_1$ amorphous ribbon. They have observed decreasing number of air pockets due to the enhancement of heat transfer coefficient at the melt-wheel interface with increasing production velocity.

### 3.5 Mössbauer spectrometry

As-quenched state

Room temperature Mössbauer spectra recorded in transmission geometry accompanied by their corresponding distributions - probabilities $P(B)$, are depicted in Fig. 6. The spectra exhibit well separated six broad absorption lines which are characteristic for fully amorphous ferromagnetic material. They we were evaluated using

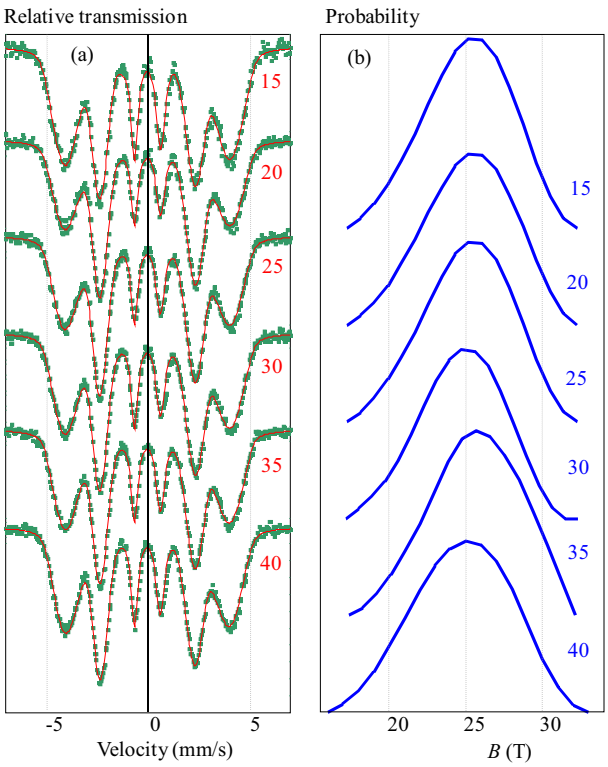


**Fig. 6.** (a) — room temperature transmission $^{57}$Fe Mössbauer spectra and (b) — corresponding hyperfine magnetic field distributions - probability $P(B)$ of the as-quenched $Fe_{78}Si_9B_{13}$ MGs prepared with the indicated velocities (m/s) of the quenching wheel

hyperfine magnetic field distributions $P(B)$. It is noteworthy that in the analysis of the Mössbauer spectra we took into consideration also the results of XRD measurements. They suggest full amorphicity of the investigated ribbons with one exception that was discussed above. Nevertheless, the amount of crystalline phase which was found at the wheel side of the 15 m/s ribbon is below the detection limit of Mössbauer spectrometry. To check for possible occurrence of crystallites in the near surface regions we have performed CEMS experiment which will be discussed below.

According to Fig. 6(a) the line width generally increases from the inside pair $(3, 4)$ to the outside pair $(1, 6)$ of absorption lines in all samples indicating the importance of field fluctuations which tend to dominate in the outer lines [2]. The spectra are smooth, *ie* no structures like shoulders are present within the lines themselves. The spectra also exhibit line width and line intensity asymmetries which are also typical for metallic glasses. Relatively large line widths are a consequence of the distribution of hyperfine interactions. In addition, as can be seen from Fig. 6(a), the intensities of the second and fifth lines systematically decrease towards higher production velocity indicating that the magnetic moments tend to orient themselves out of the ribbon plane. Nevertheless, a deviation from this pattern is observed in case of 15 m/s.

In order to monitor spin texture in the specimens, an $A_{23}$ parameter that put into ratio the intensities (areas) of the 3$^{rd}$ and 4$^{th}$ lines to the 2$^{nd}$ and 5$^{th}$ ones was used for quantification. $A_{23}$ equals to 4 in the absence of any stresses in the specimen since all atomic spins are expected to remain within the ribbon plane (due to shape anisotropy). On the other hand, for completely random spin alignment $A_{23} = 2$. The value of $A_{23} = 0$ means that the spins are perpendicular to the ribbon plane [1, 3]. Variation of the average values of the hyperfine magnetic fields $< B >$ and $A_{23}$ as a function of the production velocity are illustrated in Fig. 7. The magnetic moments are widely spread in the as-cast $Fe_{78}Si_9B_{13}$ amorphous ribbons. Consequently, a complex anisotropy distribution caused by the internal stresses induced during the quenching process is observed in Fig. 7(a) by notable deviations in $A_{23}$ parameters namely at the low production velocity region.

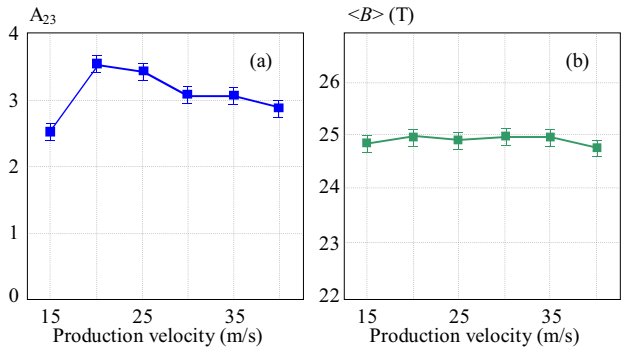


**Fig. 7.** Plot of (a) — $A_{23}$, and (b) — the average hyperfine magnetic field $< B >$) against the production velocity for the as quenched samples

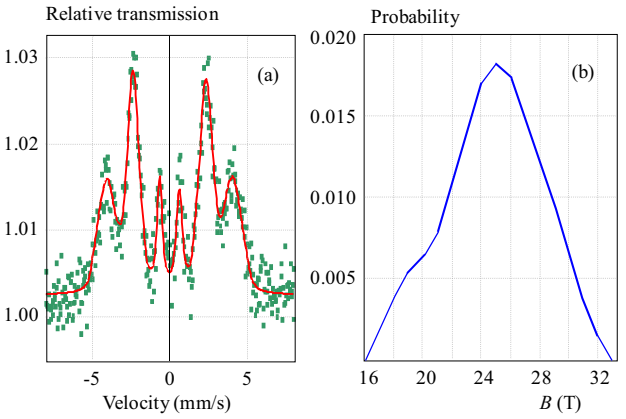


**Fig. 8.** (a) — CEMS spectrum taken from the wheel side, and (b) — corresponding hyperfine magnetic field distribution - probability $P(B)$) of the as-quenched $Fe_{78}Si_9B_{13}$ MG prepared with 15 m/s

On the other hand, the average hyperfine magnetic fields plotted in Fig. 7(b) are stable over the entire range of production velocities. This means that the average hyperfine magnetic field does not depend upon the thickness of the ribbons though orientation of the particular magnetic moments is considerably affected.

Because transmission Mössbauer spectra have not revealed any traces of crystalline phases in the bulk of the ribbon, we have performed CEMS which scans the surface regions. As an example, CEMS spectrum taken from

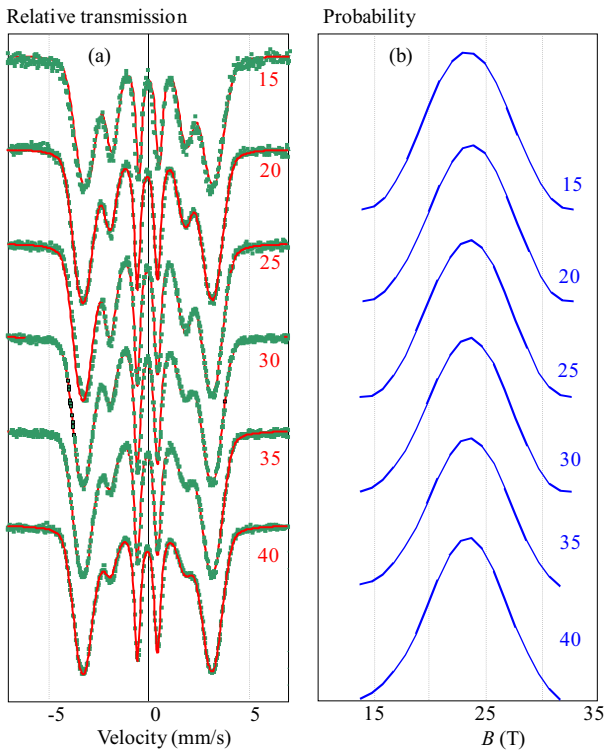


**Fig. 9.** (a) — transmission Mössbauer spectra and corresponding distributions of hyperfine magnetic fields - probability $P(B)$, and (b) — of annealed samples at 450 °C for 60 min. The particular preparation velocities are indicated in the figure (in m/s)

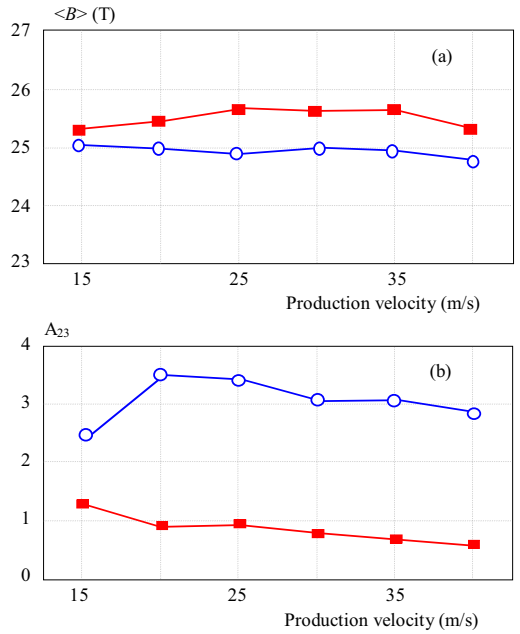


**Fig. 10.** (a) — average hyperfine magnetic field $< \mathrm{B} >$ and (b) — $A_{23}$ plotted against the production velocity. The symbols blue open circle and red solid square represent the as-quenched and the annealed states, respectively.

the wheel side of the as-quenched $Fe_{78}Si_9B_{13}$ ribbon prepared with the velocity of 15 m/s is shown in Fig. 8 together with the corresponding $P(B)$ distribution. As it can be seen this sample exhibits no apparent signs of narrow lines which could indicate presence of crystallites as follows from the XRD results. This is possibly due to very low crystalline content. Moreover the expected Mössbauer spectral lines are completely overlapped with a broad sextuplet from the amorphous matrix.

Since the wheel side is in direct contact with the rotating wheel, quenching rate of the solidification process is faster than that in the bulk [16]. Consequently, we can expect some differences between surface and bulk hyperfine parameters. The average $^{57}$Fe hyperfine magnetic field in the bulk as-quenched state of the 15 m/s sample is $24.88 \pm 0.13$ T, while that of the corresponding ribbon surface is $24.84 \pm 0.13$ T. So we can conclude that the local iron atoms environments are practically unchanged.

Nevertheless, as far as orientation of the magnetic moments positioned in bulk and on the surface of the ribbons is concerned, the bulk shows close-to-random arrangement of the moments $A_{23} = 2.48$ whereas the surface is highly textured $A_{23} = 3.83$. Surface magnetic moments are oriented close to the ribbon plane, *ie* perpendicular to the Mössbauer $\gamma$-ray direction.

Annealed state

The transmission Mössbauer spectra in Fig. 9 were taken at room temperature after annealing the samples at 450 °C for 60 min. They show a dramatic collapse of the second (or fifth) line intensities towards higher preparation velocities. It is obvious that during the annealing process, the ferromagnetic state is conserved. On the other hand, no crystalline phases were identified as the temperature of annealing was lower than the onset of crystallization.

As expected the mean hyperfine magnetic fields and hence the hyperfine magnetic moments increased after the annealing in comparison with the as-quenched state as demonstrated in Fig. 10(a). The average values of $(24.9 \pm 0.2)$ T and $(25.4 \pm 0.2)$ T for the as-quenched and annealed states, respectively, are quite close one to another. Also this quantity is practically independent on the production velocity within the error range. On the other hand, the parameter $A_{23}$ which is related to the relative areas of the 2$^{\mathrm{nd}}$ and the 5$^{\mathrm{th}}$ Mössbauer lines is higher in the as-quenched samples than in the annealed ones. It suggests that the net magnetization is positioned closer to the ribbon plane in the as-quenched state. The observed changes in $< \mathrm{B} >$ and $A_{23}$ can be related to temperature induced structural rearrangements that take place within the amorphous matrix.

## 4 CONCLUSIONS

The effect of quenching wheel velocity in the melt spinning method upon some properties of $Fe_{78}Si_9B_{13}$ MG was investigated. Varying the quenching wheel velocity, ribbons with different thicknesses were produced. SEM results confirmed that the quenching rate affects the sample morphology. XRD measurements as well as $^{57}$Fe Mössbauer spectrometry studies indicated amorphous nature of the produced ribbons with one exception. At the

wheel side of the ribbon prepared with the lowest velocity namely 15 m/s, presence of small amounts of $Fe_3Si$ crystallites was unveiled by XRD. Mössbauer experiments performed in transmission geometry as well as using conversion electrons emitted from near surface regions have not confirmed these findings most probably because of the detection limits.

Average hyperfine magnetic fields of the samples in the as-quenched state and after annealing do not exhibit substantial deviations with the production velocity and they are almost equal within the experimental error range. Though, after annealing slightly higher values of $< B >$ are observed. On the other hand, the $A_{23}$ parameters suggest a tendency of the magnetic moments to turn out of the ribbon plane after annealing.

We can conclude that after annealing the magnetic anisotropy improves which is indicated in the corresponding Mössbauer spectra by an increase in the average hyperfine magnetic field values and stabilization of the position of the net magnetic moment.

**Acknowledgement**

This work was supported by the grants GACR 14-12449S, and VEGA 1/0182/16. We thank P. Novak (Bratislava) for providing the XRD measurements.

## References

[1] KUZMANN, E.—STICHLEUTNER, S.—SÁPI, A.—VARGA, L. K.—HAVANCSÁK, K.—SKURATOV, V.—HOMONNAY, Z.—VÉRTES, A.: Hyperfine Interactions **207** (2012), 73.

[2] BHATNAGAR, A. K.: Hyperfine Interactions **25** (1985), 637.

[3] LI, X.—ZHANG, K.—WANG, C.—HAN, W.—WANG, G.: J. Mater. Sci. Technol. **23** (2007), 253.

[4] JAKUBCZYK, E.: Materials Science-Poland **24** (2006), 1027.

[5] OK, H. N.—MORRISH, A. H.: Phys. Rev. B **22** (1980), 3471.

[6] OK, H. N.—MORRISH, A. H.: J. Phys. F **11** (1981), 1495.

[7] KRAUS, L.—ZIVOTSKY, O.—POSTAVA, L.—SVEC, P.—JANICKOVIC, D.: IEEE Trans Magn. **44** (2008), 3875.

[8] LEU, M. S.—CHIN, T. S.: In: MRS Proceedings (M. Coey, L.H. Lewis, B-M. Ma, T. Schrefl, L. Schultz, J. Fidler, V.G. Harris, R. Hasegawa, A. Inoue, M.E. McHenry, eds.), Cambridge, England, 1999, p. 557.

[9] JAKUBCZYK, E.—KRAJCZYK, A.—JAKUBCZYK, M.: Journal of Physics **79** (2007), 12008.

[10] CADOGAN, J. M.—CAMPBELL, S. J.—JING, J.—FOLEY, C. P.—KATER, P.—MAI, Y. W.: Hyperfine Interact **226** (2014), 7.

[11] KANE, S. N.—GUPTA, A.—VARGA, L. K.: J. Magn. Magn. Mat. **254-255** (2003), 501.

[12] MENG, L. L.—LI, X. Y.—PANG, J.—WANG, L.—AN, B.—YIN, L. J.—SONG, K. K.—WANG, W. M.: Journal of Metallurgical and Materials Transitions A **44A** (2013), 5122.

[13] BRAND, R. A.: NORMOS programs, Universitaet Duisburg, Germany (1987).

[14] QIN, J.—GU, T.—YANG, L.—BIAN, X.: Appl. Phys. Lett. **90** (2007), 201909-2.

[15] SOHRABI, S.—ARABI, H.—BEITOLLAHI, A.—GHOLAMIPOUR, R.: Journal of Materials Engineering and Performance **22** (2013), 2185.

[16] ROGALSKI, M. S.—BIBICU, I.: Phys. Status Solidi B **195** (1996), 531.

Received 15 July 2016

**Narges Amini**, born in 1986 in Marivan, Iran, studies in a PhD course at the Physics department, Faculty of Science, Bu-Ali Sina University since 2012. She has cooperation with the Slovak University of Technology, Faculty of Electrical Engineering and Information Technology. Her thesis includes investigations of Fe-based amorphous alloys with emphasis on their magnetic properties using different tools especially Mössbauer spectrometry, XRD, VSM, etc. She focuses on crystallization behaviour and the effects of nanograins from the technical application point of view.

**Július Dekan** (Ing, PhD), born in 1980 in Bratislava, Slovakia, graduated from the Faculty of Electrical Engineering and Information Technology, Slovak University of Technology in Bratislava in branch Electromaterial Engineering and received the PhD degree in Physical Engineering in 2010. Since 2008, works as a researcher specialized in Mössbauer spectrometry at the Institute of Nuclear and Physical Engineering (formerly Department of Nuclear Physics and Technology).

**Milan Pavúk** (Ing, PhD), born in Bratislava in 1980. He obtained his doctoral degree in the field of Physical Engineering at the Faculty of Electrical Engineering and Information Technology, Slovak University of Technology in Bratislava in 2010. Since 2008, he has been working as a researcher at the Institute of Nuclear and Physical Engineering at the same university. He specializes in Atomic Force Microscopy, Magnetic Force Microscopy, and studying surface properties of solid matters in general.

**Safdar Habibi**, born in 1957 in Tehran, Iran, obtained his PhD in solid state physics in 1991 from Devi Ahylia University, Indore India. His field of interest is mainly study of magnetic and mechanical properties, the short range order in amorphous metallic alloys specially those of Iron based, nanocrystalline materials. He uses different tools such as Mossbauer spectroscopy, XRD, VSM and microhardness for this purpose. At present he is a lecturer in Physics Department, Bu Ali Sina University, Hamedan, Iran.

**Marcel Miglierini** (Prof, Ing, DrSc) born in 1956 in Bratislava, Slovakia, graduated from the Slovak University of Technology in Bratislava where he has received the DrSc degree (1995) and was appointed as a full professor (1997). He is a specialist in Mössbauer spectrometry applied namely to disordered systems. His recent activities comprise the use of synchrotron radiation for investigations of nuclear resonances.